PHILOSOPHICAL TRANSACTIONS OF THE ROYAL SOCIETY B BIOLOGICAL SCIENCES

Modelling avian biodiversity using raw, unclassified satellite imagery

Véronique St-Louis, Anna M. Pidgeon, Tobias Kuemmerle, Ruth Sonnenschein, Volker C. Radeloff, Murray K. Clayton, Brian A. Locke, Dallas Bash and Patrick Hostert

Phil. Trans. R. Soc. B 2014 **369**, 20130197, published 14 April 2014

PHILOSOPHICAL TRANSACTIONS OF THE ROYAL SOCIETY B

rstb.royalsocietypublishing.org

Research

Cite this article: St-Louis V, Pidgeon AM, Kuemmerle T, Sonnenschein R, Radeloff VC, Clayton MK, Locke BA, Bash D, Hostert P. 2014 Modelling avian biodiversity using raw, unclassified satellite imagery. *Phil. Trans. R. Soc. B* **369**: 20130197. http://dx.doi.org/10.1098/rstb.2013.0197

One contribution of 9 to a Theme Issue 'Satellite remote sensing for biodiversity research and conservation applications'.

Subject Areas:
ecology

Keywords:
avian habitat modelling, biodiversity conservation, Chihuahuan Desert, image texture, spectral mixture analysis, landsat

Author for correspondence:
Véronique St-Louis
e-mail: veronique.st-louis@state.mn.us

†Present address: MNDNR Wildlife Biometrics Unit, 5463-C West Broadway, Forest Lake, MN 55025, USA.

Royal Society Publishing

Modelling avian biodiversity using raw, unclassified satellite imagery

Véronique St-Louis[1,†], Anna M. Pidgeon[1], Tobias Kuemmerle[1,2], Ruth Sonnenschein[2], Volker C. Radeloff[1], Murray K. Clayton[3], Brian A. Locke[4], Dallas Bash[4] and Patrick Hostert[2]

[1]Department of Forest and Wildlife Ecology, University of Wisconsin-Madison, Madison, WI, USA
[2]Geography Department, Humboldt-Universität zu Berlin, Berlin, Germany
[3]Department of Statistics, University of Wisconsin-Madison, Madison, WI, USA
[4]Directorate of Environment, Fort Bliss, TX, USA

Applications of remote sensing for biodiversity conservation typically rely on image classifications that do not capture variability within coarse land cover classes. Here, we compare two measures derived from unclassified remotely sensed data, a measure of habitat heterogeneity and a measure of habitat composition, for explaining bird species richness and the spatial distribution of 10 species in a semi-arid landscape of New Mexico. We surveyed bird abundance from 1996 to 1998 at 42 plots located in the McGregor Range of Fort Bliss Army Reserve. Normalized Difference Vegetation Index values of two May 1997 Landsat scenes were the basis for among-pixel habitat heterogeneity (image texture), and we used the raw imagery to decompose each pixel into different habitat components (spectral mixture analysis). We used model averaging to relate measures of avian biodiversity to measures of image texture and spectral mixture analysis fractions. Measures of habitat heterogeneity, particularly angular second moment and standard deviation, provide higher explanatory power for bird species richness and the abundance of most species than measures of habitat composition. Using image texture, alone or in combination with other classified imagery-based approaches, for monitoring statuses and trends in biological diversity can greatly improve conservation efforts and habitat management.

1. Introduction

The current global biodiversity crisis requires the accurate and efficient mapping and monitoring of broad-scale patterns of biodiversity. Developing methods for effectively monitoring status and trends in biodiversity is necessary to understand pressures encountered by biodiversity, and consequent responses. Remotely sensed data are increasingly used to model and understand species distributions in space and time [1–4]. The challenge is how to quantify habitat features that are ecologically relevant to the species, or guilds, of interest given the potential mismatch between the spatial resolution of satellite images and individuals' perception and utilization of habitat. This mismatch is exacerbated by the fact that (i) images are commonly classified into discrete land cover classes, thus ignoring subtle variations within a given class and gradients between classes, (ii) the spatial resolution (i.e. pixel size) may be inadequate to capture habitat of interest, and (iii) changes in phenology may affect whether or not certain habitat attributes are detected by the sensors. To address the first and second of these shortcomings, we evaluated the usefulness of two remotely sensed approaches that capture wildlife habitat features, i.e. image texture and spectral mixture analysis (SMA), in avian habitat models. Image texture captures among-pixel habitat heterogeneity, while SMA captures the proportion of different habitat components within a given pixel. Both approaches address the need for remote sensing-based methods that detect within-habitat subtleties when mapping and monitoring on-the-ground biological diversity [5–7].

Approaches for mapping and monitoring broad-scale patterns of biodiversity need to be focused towards the ecological requirements of the

species or groups of species of interest. Models aimed at predicting avian species richness, for example, need to include measures of (i) habitat heterogeneity (i.e. horizontal and vertical variability in habitat features) and (ii) productivity (i.e. amount of green biomass), two of the main correlates of biodiversity [8]. However, if the goal is to model the abundance of birds, then using features that capture the amount of suitable habitat (i.e. habitat composition) may be more relevant than measures of habitat heterogeneity. Birds, in particular, respond to a variety of habitat features, and capturing the full breath of those features using remotely sensed data is challenging.

Building habitat models to map and monitor biodiversity is particularly challenging, especially in semi-arid ecosystems where fine-scale variability within a given land cover class is often high. The segregation of continuous landscapes into discrete land cover classes, an approach typically used to model biodiversity using remotely sensed data, may overlook subtle variations in habitat components within a given land cover class that are relevant to wildlife species, such as vegetation composition and structure. Within-pixel variation is also ignored [9]. Pixels are often composed of a mixture of habitat classes [10] that may not all be relevant to a species. In addition to exhibiting high within-habitat heterogeneity, semi-arid ecosystems sometimes have gradual transitions between some habitat types, which may lead to low classification accuracy. In semi-arid and arid ecosystems especially, using continuous rather than discrete data is advantageous (e.g. in Mediterranean ecosystems [11], the Indian subcontinent [12], urban centres of the desert United States and sub-Saharan Africa [13,14]). Indeed, our previous analyses conducted in a semi-arid ecosystem of New Mexico showed that habitat features derived from unclassified imagery, i.e. image texture and the Normalized Difference Vegetation Index (NDVI), were superior to landscape indices obtained from a classified image for explaining bird species richness [15]. Whereas measures of habitat heterogeneity calculated from raw imagery explained up to 87% of the variability in bird species richness, landscape indices explained 55% only.

In general, image texture has high potential for predicting habitat in models, and thus improving upon methods for mapping and monitoring biodiversity. Image texture of remotely sensed images has traditionally been used to improve image classification [16–20]. The habitat classes created by such a classification can, in turn, be used for mapping habitat, for example, for grasshopper sparrows (*Ammodramus savannarum*) in Canada [21]. Image texture can also improve wildlife habitat models directly. For example, image texture of the NDVI is positively associated with the abundance of bird species requiring heterogeneous habitats (e.g. song sparrow (*Melospiza melodia*), yellow warbler (*Dendroica petechia*) and black-throated green warbler (*Dendroica virens*) in Maine [22], and grasshopper sparrows in Wisconsin [7]). In Argentina, image texture substantially improved habitat models for the endangered greater rheas (*Rhea americana*) [23]. Texture also performs well for modelling species richness [15,24] because of the theoretical positive relationship between the number of species and habitat heterogeneity [25]. These examples show the potential of image texture to improve upon approaches that are based on image classification when mapping and monitoring biological diversity in diverse habitat types.

Another challenge of remote sensing analysis for the purpose of mapping and monitoring biodiversity is to measure features that capture fine-scale habitat composition. Image pixels contain potentially useful habitat information that cannot be extracted with traditional image classification methods, or by image texture analysis. SMA (also called 'spectral unmixing'), on the other hand, decomposes pixel reflectance values into different habitat components (e.g. green vegetation, soil and dry vegetation), thereby alleviating the assumption of image classification methods that each pixel is composed of only one habitat component. Spectral unmixing assumes that the reflectance information contained within each image pixel is the linear combination of the pure reflectance of many components [26]. Using pure reflectance spectra, spectral unmixing can quantify the percentage cover of varying habitat components across a range of dryland ecosystem types from sand dunes [10] to Mediterranean shrublands [27,28]. Habitat components with very high spectral contrast (e.g. green vegetation and soil) can be particularly well assessed [10]. Quantifying the proportion of green vegetation in a given area using spectral unmixing is thus promising for characterizing bird habitat, especially in ecosystems where vegetation indices may be less reliable owing to strong soil background, such as semi-arid ecosystems [29,30]. However, SMA has rarely been used to model wildlife habitat, although a few examples exist. Habitat selection models for the mountain bongo (*Tragelaphus euryceros*) based on spectral unmixing performed better than those based on field or remotely sensed data alone [31]. Spectral unmixing fractions explain 84% of the variability in urban bird species richness in Israel (in combination with other geographical variables such as distance to roads) [32]. Similarly, soil and shadow fractions successfully characterize hooded warbler (*Wilsonia citrine*) nest sites in Ontario, where the first two principal components of all the unmixing fractions and texture measures capture 95.9% and 88.3% of the variance in nest site locations, respectively [33]. Because of the high performance of SMA in semi-arid ecosystems, we wondered whether it would be a good alternative or complement to image texture for predicting bird abundance in the Chihuahuan Desert of New Mexico, and potentially a valuable tool to monitor the status of and predict trends in biological diversity over time in different habitat types.

The overall goal of our study was to compare the relative ability of image texture, a measure of among-pixel heterogeneity, and SMA, a measure of within-pixel habitat composition, for explaining bird species richness and the abundance of 10 bird species that breed in a semi-arid ecosystem of New Mexico. The comparison of these two approaches is novel, and in addition to informing which methodology may be best for explaining patterns of species distribution in semi-arid landscapes, it may also provide insights into which environmental cues, related to either heterogeneity of habitats or composition, species most respond to in these types of landscapes. Because of the strong theoretical relationship between species biodiversity and habitat heterogeneity [8], we hypothesized that species richness would be best explained by among-pixel measures of habitat heterogeneity. On the other hand, we hypothesized that the abundance of species would be best explained by measures derived from spectral unmixing that capture within-pixel habitat composition, because they may quantify subtle changes in habitat components relevant for different species' unique life-history requirements.

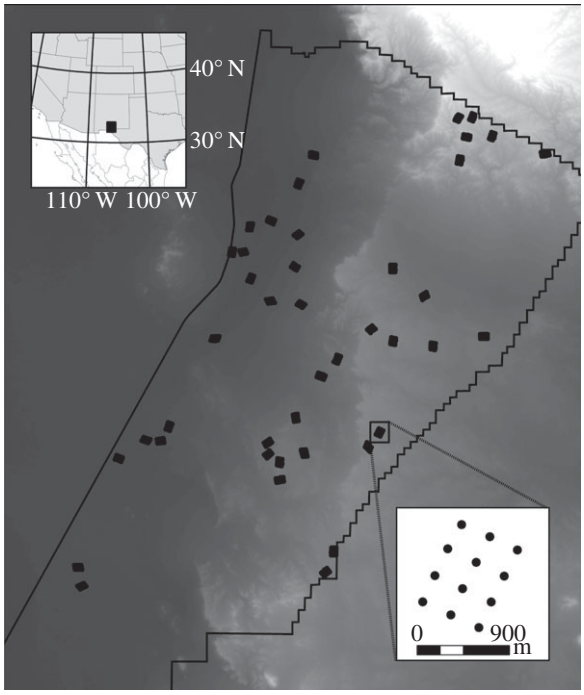

Figure 1. Location of the McGregor range of the Fort Bliss military base in New Mexico overlayed on a 10 m DEM (elevation values range from 569 m (dark grey) to 3629 m (white). The black dots indicate the location of the 42 study plots, and the small bottom-right insert shows the details of one of the 42 108 ha study grids.

2. Material and methods

(a) Study area

Our study was conducted in the northern Chihuahuan Desert, specifically on almost 300 000 ha of Fort Bliss Army Reserve in New Mexico (figure 1). The area is semi-arid, with monthly precipitation ranging between 13 and 44 mm from May to July, minimum temperatures between 11 and 19°C, and maximum temperatures between 30 and 35°C (Western Regional Climate Center. Orogrande 1N New Mexico). The study area contains multiple habitat types including two grassland types (black grama (*Boutela eriopoda*) and mesa grassland), four shrubland types (creosote (*Larrea tridentata*), mesquite (*Prosopis glandulosa* or *P. pubescens*), sandsage (*Artemisia filifolia*), and whitethorn (*Acacia neovernicosa* or *A. constricta*)), and one low tree-dominated habitat, pinyon–juniper (*Pinus edulis–Juniperus monosperma* or *J. deppeana*). For a more detailed description of the plant associations occurring in the area, refer to Pidgeon *et al*. [34,35]. The field sites were represented by different soil types according to a digital soil map [36], including deep sand, draw, gravel, gyp upland, limestone hills, limy, loamy, sandstone hill and sandy.

(b) Bird data

Bird abundance was summarized over forty-two 12-point plots (108 ha each) placed randomly across the seven habitat types presented above (figure 1). Four to five visits per year were conducted at each point count during the 1996–1998 breeding seasons. All individuals heard or observed within 150 m of the points and during a 10 min period were recorded. Based on these data, we summed the counts per plot of a given species to obtain plot-level species abundance data. We summarized abundances for 10 species with different habitat associations and life-history characteristics (table 1). Because distances were not recorded when we collected our field data, back in 1996–1998, we do not have the appropriate distance estimates to apply a distance-sampling approach. We used only presence–absence data for three out of the 10 species (eastern meadowlark, scaled quail and verdin) because they were found in low numbers and on a relatively few sites. For these three species, we recorded the presence at a given location if an individual of that species was detected at any of the point counts in a given season. Species richness was calculated as the sum of all species detected at any of the point counts at each plot.

(c) Image pre-processing

We selected the satellite images that matched the time period of bird observations best. Two Landsat Thematic Mapper 5 (TM5) images from the same path, and recorded on the same day (path/row 33/37 and 33/38 of 25 May 1997) were used. We used images from 1997 only because available images for the two other years of bird data collection (i.e. 1996 and 1998) were too cloudy to be analysed successfully. We used a two-stage process to convert raw digital numbers into surface reflectances [37]. First, we applied TM calibration gains and biases [38,39] to calculate at-satellite radiance values. Second, we used an atmospheric transfer model that considered terrain illumination to convert at-sensor radiance to surface reflectance [40]. As a topography model, we used a 10 m resolution digital elevation model (DEM) and re-sampled it to 30 m TM resolution. We assumed a continental, clear sky atmosphere and iteratively changed water vapour content and aerosol distribution parameters until image spectra matched reference spectra of (i) soils, (ii) clear water and (iii) white gypsum sand. We collected a total of 36 soil samples in the field during summer 2007, and measured these in the laboratory using an ASD Fieldspec Pro II spectroradiometer. We obtained a white sand reference spectrum from the ASTER library [41] and a clear water spectrum from the Erdas [42] Imagine spectral library. All reference spectra were re-sampled to Landsat TM5 bands. We selected pure image spectra to compare with the reference spectra from the Landsat TM images based on digital orthophotos quarter quadrangles and a soil map in vector format. We quantified differences of reference and image spectra using the root mean square error (RMSE) and the coefficient of determination (R^2; 0.99 for red soils, 0.95 for grey soils, 0.89 for white sand and 0.78 for water).

(d) Among-pixel habitat heterogeneity

We calculated among-pixel habitat heterogeneity based on image texture of the NDVI (a measure of photosynthetically active green vegetation). Our previous work showed that NDVI texture is superior to the texture of any individual Landsat TM band for predicting avian biodiversity in this ecosystem [15]. Texture measures were calculated in a fixed (rather than moving) 9×9 window around each point count location. We calculated plot-level texture by averaging the 12 texture values corresponding to the 12 point count locations for each plot. We opted for a 9×9 window to approximate the spatial extent of the 150 m radius point counts (approx. 7 ha). We selected one first-order, and three second-order texture [16] measures for quantifying texture at each plot. The measure of first-order standard deviation was selected because of its intuitive appeal for characterizing zones of higher or lower heterogeneity. As many of the second-order measures are correlated with each other [24], we selected only two for this analysis (angular second moment and correlation), based on ease of interpretation. Angular second moment and correlation emphasized areas that were homogeneous in terms of NDVI values.

Image texture can also be calculated based on the SMA results, i.e. using the green vegetation fraction as a measure of green biomass instead of NDVI or any other individual band. However, a preliminary analysis suggested that texture of SMA fraction was not better at explaining bird abundance and

Table 1. List of species and guild affiliation. Italic indicates instances where a species was the most abundant for that particular guild, based on total counts compiled across all 42 study sites.

species	AOU code	breeding guild	foraging guild	nesting guild
ash-throated flycatcher *Myiarchus cinerascens*	ATFL	shrub	lower/air	trees/shrubs
black-headed grosbeak *Pheucticus melanocephalus*	BHGR	wood	*upper*	trees/shrubs
black-throated sparrow *Amphispiza bilineata*	BTSP	*shrub*	*ground*	*ground*
cactus wren *Campylorhynchus brunneicapillus*	CACW	shrub	ground	ground
common bushtit *Psaltriparus minimus*	COBU	shrub	upper	trees/shrubs
eastern meadowlark *Sturnella magna*	EAME	*grass*	ground	ground
Scott's oriole *Icterus parisorum*	SCOR	shrub	*lower*	*trees/shrubs*
scaled quail *Callipepla squamata*	SCQU	grass	ground	ground
spotted towhee *Pipilo maculatus*	SPTO	*wood*	air	trees/shrubs
verdin *Auriparus flaviceps*	VERD	shrub	lower	trees/shrubs

occurrence than texture of NDVI (results not shown). For this reason, we only present results obtained based on NDVI texture.

(e) Within-pixel habitat composition

We calculated within-pixel habitat composition using SMA. SMA assumes that most of the variation in the reflectance of a pixel can be attributed to a limited number of surface materials which can be characterized by pure reflectance spectra (hereafter, endmembers) [43]. Assuming that any image pixel spectrum is the linear combination of the endmember spectra (e.g. vegetation, soil, rock, plus an unexplained residual error), SMA decomposes image pixel spectra into endmember fractions. These fractions can then be interpreted as the relative proportion of a pixel's surface covered by the respective surface class (e.g. vegetation, soil) [28].

The endmembers can be derived from the image itself, or from samples measured in the field or in the laboratory. We used laboratory spectra as the highly heterogeneous landscape does not easily allow identification of pixels containing only a single endmember. We compiled a spectral library with four different categories of endmember spectra: (i) photosynthetically active vegetation (hereafter, green vegetation), (ii) photosynthetically inactive vegetation (hereafter, dry vegetation), (iii) soil and (iv) shade. Soil and dry vegetation samples were acquired in the field in summer 2006, and measured in the laboratory using the ASD Fieldspec Pro II spectroradiometer. We obtained green vegetation spectra from the United States Geological Survey (USGS) spectral library [44], and from a library of sample spectra collected in semi-arid and Mediterranean environments in Greece [30]. The latter contained both reference spectra measured in the laboratory (leaves only) and integrated spectra gathered in the field (leaves, branches and stems).

To estimate the fraction of green vegetation, dry vegetation, soil and shade, we fitted three- and four-endmember models in a multiple endmember spectral mixture analysis (MESMA). In MESMA, the number of endmembers (three or four in our case) can vary on a per-pixel basis to achieve the optimal decomposition [27]. This approach assumes that models of higher dimensions are picked because they represent on-the-ground landscape features better than models of lower dimension, and that the better fit is not only the statistical result of a higher degree of freedom. The spectra used for characterizing these endmembers can also vary (e.g. several green vegetation spectra are available alternatively as a green vegetation endmember). We set a maximum of four endmembers owing to the low dimensionality of Landsat TM data [45]. For each pixel, the spectral reflectance values could thus be represented by a linear combination of (i) green vegetation, soil and shade, (ii) dry vegetation, soil and shade or (iii) green vegetation, dry vegetation, soil and shade. SMA uses a least-squares regression approach to obtain the best fit between the reference spectra and the estimated SMA fractions. Out of the three aforementioned models, the linear combination that resulted in the lowest RMSE was retained for providing the fractions of green and/or dry vegetation, and the fractions of soil and shade. The RMSE for each pixel was also recorded as a separate data layer to visualize the spatial pattern of fit between the modelled fractions and the reference spectra.

The spectral unmixing was conducted with different spectra for characterizing green vegetation, dry vegetation and soil. Ultimately, we selected a set of spectra that generated good results based on the minimum overall RMSE (calculated as the average RMSE of all pixels in the image). The model that achieved the best endmember decomposition (i.e. lowest RMSE) was based on an integrated vegetation spectrum from Crete (i.e. from a spectrum collected in the field that incorporates green leaves as well as branches), as well as dry grasses and soils spectra from our New Mexico study area. The spectral unmixing was performed using the tool VMESMA [46].

We normalized the fractions of green vegetation, dry vegetation and soil by redistributing the amount of shade proportionally to the fractions of the other habitat components. For example, if a pixel had 20% soil, 30% dry grass, 40% green vegetation and 10% shade, the normalized fractions obtained by redistributing the 10% shade would be 22.22% soil, 33.33% dry grass and 44.44% green vegetation.

Green and dry vegetation fractions were summarized as the average fraction within a 9×9 window around each point-count point. We averaged the resulting values across the 12 points to obtain plot-level values. In addition to NDVI texture and SMA fractions, we extracted elevation at each point count from the

10 m DEM and averaged it for each plot to account for the effect of elevation on the spatial distribution of birds in the statistical models of bird abundance or occurrence.

(f) Statistical analyses

We conducted the statistical analyses using only 38 of the 42 study plots because four plots were partially covered by clouds in the satellite image. We used regression models to (i) evaluate whether NDVI texture and SMA fractions significantly explained abundance, occurrences and species richness, (ii) identify whether NDVI texture or SMA better explained species abundance or occurrence and species richness, and (iii) evaluate which texture and SMA variables have the highest explanatory power. First, we fitted each possible combination of (i) texture measures and (ii) SMA fractions to explain the abundance or occurrence of birds and bird species richness. For seven of the 10 species and for species richness (i.e. excluding eastern meadowlark, scaled quail and verdin for which we only used presence–absence data), we square-root transformed the counts, and used a linear model with Gaussian error structures. While Poisson models are also appropriate for modelling counts, the statistical modelling approach that we used required valid likelihoods to perform Bayesian model averaging (explained below). The likelihoods obtained using mixed-effect Poisson models would not have been valid to conduct such an analysis, which is why we used transformed data and Gaussian models as opposed to Poisson. Because of the repeated visits of each plot during a breeding season, we fitted mixed-effect models using plot as a random effect and included Julian day within a given year in the list of potential covariates in the models. In addition, we tested for temporal autocorrelation by comparing models fitted with or without an autoregressive correlation structure of order 1 (AR1) using a likelihood-ratio test. We thus included an AR1 term when it significantly improved a model. We proceeded as such for the seven species modelled with a Gaussian error structure. For eastern meadowlark, scaled quail and verdin, we analysed only presence–absence logistic regressions, i.e. generalized linear mixed effects model with a binomial error structure, because of the high number of plots in which either one or zero birds were detected.

For each fitted model, we evaluated the overall significance using a likelihood-ratio test comparing its fit to the null model (i.e. intercept only) obtained using the same random effect (when applicable) and error structure. We also extracted the Bayesian information criterion (BIC) for all models fitted with image texture and all models fitted with SMA fractions. The BIC values were used to calculate the coefficient posterior probabilities of all the variables, and to obtain model averaged coefficients using Bayesian model averaging (BMA, e.g. [47]). The posterior probabilities represent, for a given variable, the probability of the coefficient being different from zero. The higher the probability, the higher our confidence is that a variable contributes in explaining the pattern. For more general details on the approach see Raftery [48] and Link & Barker [49]. For each species, and for species richness, we calculated the difference between the BIC of the NDVI texture models, and that of the SMA fraction models (ΔBIC; table 2). Large absolute values of ΔBIC indicate that one approach performed substantially better than the other, whereas ΔBIC values close to zero (approx. 2 or smaller) indicate that the two methods performed equally well. All statistical analyses were conducted in R [50]. We fitted mixed-effect models in the nlme packages [51].

Table 2. BIC of the model with the highest posterior probability amongst all models fitted for each species/year or species richness/year combination, using the NDVI texture variables or the SMA fractions. A negative difference in BIC (ΔBIC) indicates that, for a given species or for species richness, the best NDVI texture model performed better than the best SMA fraction model. Differences larger than 4 indicate that a method was substantially better than the other.[a,b]

species	year	best NDVI texture model BIC	best SMA fraction model BIC	ΔBIC
ATFL	1996	481	493 (n.s.)	−12
	1997	395	405 (n.s.)	−10
	1998	361	369 (n.s.)	−8
BHGR	1996	255	249	6
	1997	147	152	−5
	1998	228	239	−11
BTSP	1996	542	542	0
	1997	428	431	−3
	1998	425	431	−6
CACW	1996	470	474	−4
	1997	362	365	−3
	1998	341	346	−5
COBU	1996	358	359	−1
	1997	168	177	−9
	1998	190	201	−11
EAME	1996	38	37	1
	1997	50	47	3
	1998	35	36	−1
SCOR	1996	490	500	−10
	1997	404	409	−5
	1998	400	410	−10
SCQU	1996	38	36	2
	1997	41	41	0
	1998	21	21	0
SPTO	1996	313	313	0
	1997	203	205	−2
	1998	108	110	−2
VERD	1996	43	48	−5
	1997	35	38	−3
	1998	35	45	−10
richness	1996	62	74	−12
	1997	35	72	−37
	1998	51	84	−33

[a]All models were conducted using the square-root transformed counts, with the exception of EAME, SCQU and VERD for which presence–absence data were used.
[b]Models that were not significantly better than the null model are indicated by (n.s.).

3. Results

(a) Measures of avian habitat components

The texture measures calculated based on NDVI values varied greatly across the study area (figure 2*a*) and among the main habitat types. We found the highest standard deviation in the pinyon–juniper, moderate in the shrublands and lowest values in grasslands. Inversely, pinyon–juniper habitat had

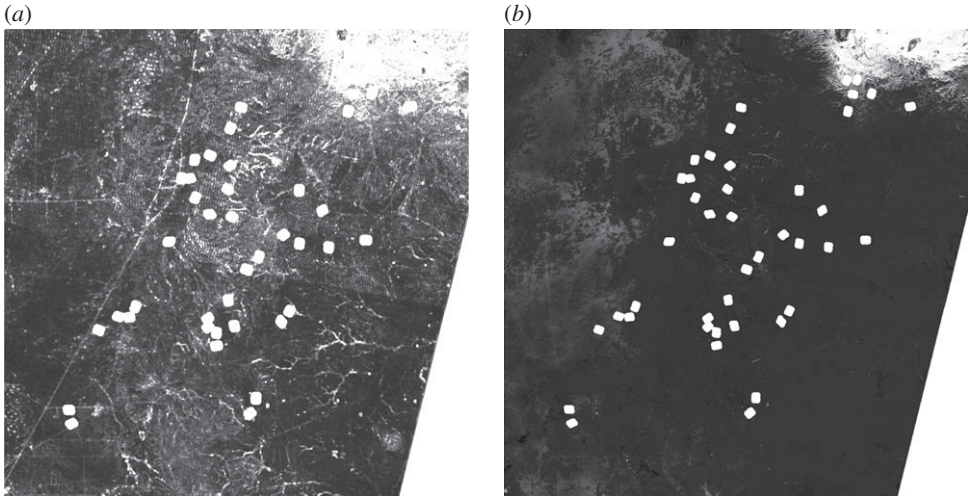

Figure 2. Comparison of NDVI texture (*a*) versus the SMA green vegetation fraction image from May 1997 (*b*). Light areas represent higher values of either texture (standard deviation of NDVI) or SMA vegetation fractions.

the lowest angular second moment and correlation (data not shown). On the other hand, plots located in the two grassland habitats had the highest angular second moment and correlation and the lowest contrast. Texture measures of the four shrubland habitats were intermediate between pinyon–juniper and the grasslands.

The SMA of the May image had a mean overall RMSE of 2.25% reflectance (figure 2*b*). Red and grey soils were very well identified, with red soils dominating mesquite sand dunes, and grey soils dominating the remainder of the study area. Green vegetation fraction, averaged across a given habitat type for the May image, was the highest in the pinyon–juniper habitat, low in the shrub habitats and close to zero in the grasslands. The fractions of dry vegetation were similar in all habitat types, but slightly lower in mesquite- and whitethorn-dominated shrublands.

(b) Modelling avian biodiversity using among-pixel heterogeneity and within-pixel composition

All models fitted using NDVI texture measures alone had significant relationships to both species richness and the abundance or occurrence of birds ($p < 0.027$) (table 2). SMA fractions also significantly explained species richness, and the abundance or occurrence of all species for all three years, with the exception of ash-throated flycatcher. For all models, we tested for and found no significant spatial autocorrelation of the residuals. The success of the models is thus not likely to be caused by spatial autocorrelation.

The large absolute value of ΔBIC indicates that NDVI texture clearly outperformed SMA fractions for modelling bird species richness (table 2). However, the difference between the two types of measures was not as marked in the models of species abundance or occurrence. Still, NDVI texture models consistently performed better than SMA fraction models across all three years for ash-throated flycatcher, cactus wren, Scott's oriole and verdin. For black-throated sparrow and common bushtit, NDVI texture models performed better than SMA fraction models for two out of the three years. Both approaches produced similar results for eastern meadowlark, scaled quail and spotted towhee.

Among the three measures of NDVI texture, angular second moment explained overall bird species richness best (figure 3*a*). There were more species in areas of high heterogeneity, indicated by low angular second moment values. The green SMA vegetation fraction had the highest posterior probabilities in the bird species richness models, along with elevation (figure 3*b*), with more species in areas with more green vegetation.

Angular second moment and standard deviation of NDVI were the two measures with the highest posterior probabilities for most species (figure 4*a*). Coefficient estimates that were significantly different than zero indicated that black-headed grosbeak, common bushtit and spotted towhee were more abundant in highly heterogeneous areas (high standard deviation and low angular second moment of NDVI values), whereas cactus wren was more abundant in areas of low heterogeneity. For species for which both the angular second moment and the standard deviation of NDVI were significant, such as for the ash-throated flycatcher and Scott's oriole, the signs of the coefficient estimates were the same, contrary to our expectation. Angular second moment and standard deviation are highly negatively correlated (Pearson correlation $= -0.85$; results not shown), indicating a potential interaction which might have affected the sign of their relationship in the multivariate model. Univariate models of ash-throated flycatcher abundance (results not shown) indicated that this species was more abundant in areas of high heterogeneity in green vegetation, while these models were not significant for the Scott's oriole.

Among the SMA fractions that we considered, the amount of green vegetation best explained the abundance or occurrence of most species (figure 4*b*). The black-headed grosbeak, common bushtit and spotted towhee were more abundant in areas of elevated green vegetation, whereas cactus wren, eastern meadowlark and Scott's oriole were associated with areas of low green vegetation.

The spatial patterns of abundance of the black-throated sparrow were better explained by elevation than by any NDVI texture measures or SMA fractions—this species was more abundant at low elevation, where the shrublands are located.

4. Discussion

Habitat models based on remotely sensed data can provide valuable information for guiding conservation strategies

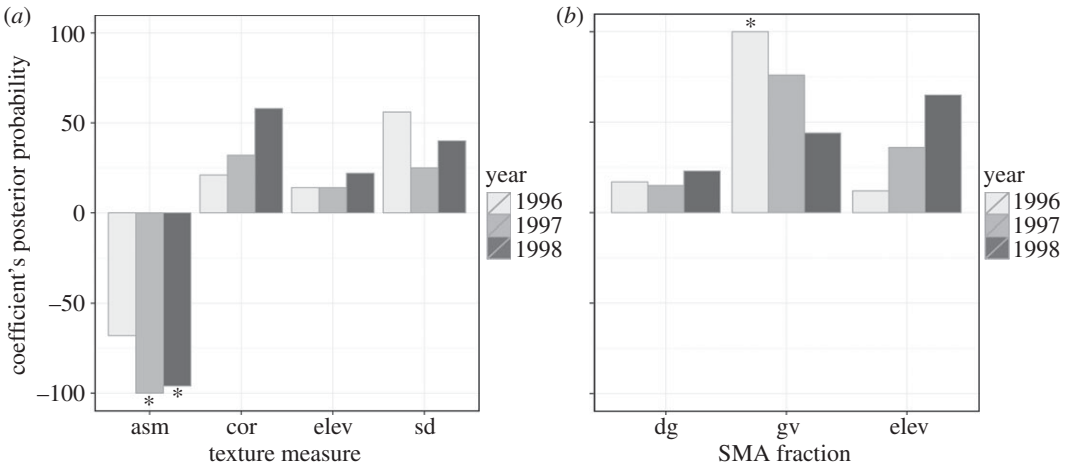

Figure 3. Coefficients' posterior probabilities obtained from the Bayesian Model Averaging of NDVI texture (*a*) and SMA fraction (*b*) covariates used to explain bird species richness at all 38 plots. The amplitude of the bars is indicative of the relative contribution of each variable for explaining the response. Stars indicate variables/year combinations for which a 95% posterior probability interval built around the corresponding BMA coefficient estimate did not include zero. Texture measures acronyms: asm, angular second moment; cor, correlation; elev, elevation; sd, standard deviation. SMA fractions acronyms: dg, dry vegetation; gv, green vegetation.

and the management of biodiversity. However, models built using satellite image classifications overlook within-habitat heterogeneity, which may be an important component of wildlife habitats. The challenge is to develop approaches to monitor species distributions over broad spatial extents based on unclassified imagery while capturing habitat features that are ecologically meaningful. Our goal was to evaluate the use of satellite-derived measures of habitat heterogeneity and habitat composition for avian habitat models in the Chihuahuan Desert of New Mexico. We hypothesized that among-pixel measures of habitat heterogeneity would best explain bird species richness, whereas within-pixel measures of habitat composition would best explain the abundance and occurrence of individual bird species. Our results showed that in our semi-arid study area, habitat heterogeneity was indeed a strong driver of species richness, and also of individual species abundance and patterns of occurrence.

Both measures of among-pixel heterogeneity (NDVI image texture) and within-pixel composition (SMA fractions) explained a substantial proportion of the variability in bird abundance and species richness, except for ash-throated flycatcher which was not significantly associated with any SMA fraction. In line with our hypothesis, we found that bird species richness models based on among-pixel heterogeneity were markedly better than those based on measures of habitat composition. However, in contrast to our hypothesis, among-pixel heterogeneity measures were also best for modelling the abundance of shrub and tree nesters including ash-throated flycatcher, black-headed grosbeak, common bushtit and Scott's oriole. We expected a strong relationship between measures of heterogeneity derived from NDVI texture and bird species richness because theory predicts higher biodiversity in areas with higher heterogeneity of resources [25,52]. Indeed, we found that heterogeneous areas accommodated more species than homogeneous areas of similar size, presumably because of a larger variety of niches in these areas.

We also expected that measures of habitat composition derived from SMA fractions would outperform measures of heterogeneity in explaining species abundance and occurrence because they capture subtleties in habitat composition within a given 30 m pixel. This expectation was not confirmed by our results; to the contrary, measures of heterogeneity were equal to—if not better than—measures of composition, in explaining the spatial distribution of most species.

Patterns of abundance of ground nesters and ground foragers were equally well explained by measures of heterogeneity or composition. However, measures of habitat heterogeneity performed best for explaining spatial patterns of tree and shrub nesters. NDVI texture appeared to have characterized the unique vertical structure of shrublands and woodlands in this ecosystem better than the SMA fractions.

Given that within-pixel measures derived from SMA fractions seldom outperformed measures of heterogeneity derived from NDVI texture in either richness or abundance or occurrence models, and given that NDVI texture is technically easier to calculate than SMA, we propose that NDVI texture is a particularly well suited measure for modelling bird abundances and bird species richness in semi-arid ecosystems. However, we note limitations of the NDVI for semi-arid ecosystems. NDVI is sensitive to soil background [53], and may produce values different from zero even for areas covered by pure rocks and soils. SMA green vegetation fractions better reflect 'true' areas of green biomass (i.e. highly productive habitats) than NDVI [29]. Interestingly though, SMA green vegetation fractions in our grasslands were close to zero, but NDVI still exhibited some variability which was quantified by image texture. Moreover, texture of SMA green vegetation fraction explained bird abundance, occurrence and species richness less well than texture of NDVI (results not shown). There is thus great potential for the use of image texture in the field of biodiversity conservation, where image texture can be used to predict the current state of biodiversity over wide areas, and assess changes in biodiversity through space and time.

Among the image texture variables, angular second moment, which measures homogeneity in pixel values [16], was the best predictor of species richness. For many species, it was also the best predictor of abundance. The relationship between angular second moment and avian patterns confirmed our expectations. Shrub and tree nesting species accordingly had a negative relationship with angular second moment. The shrublands and woodlands on which they depend during the nesting season are typically associated with more heterogeneous vegetation patterns in our study area as opposed to grasslands.

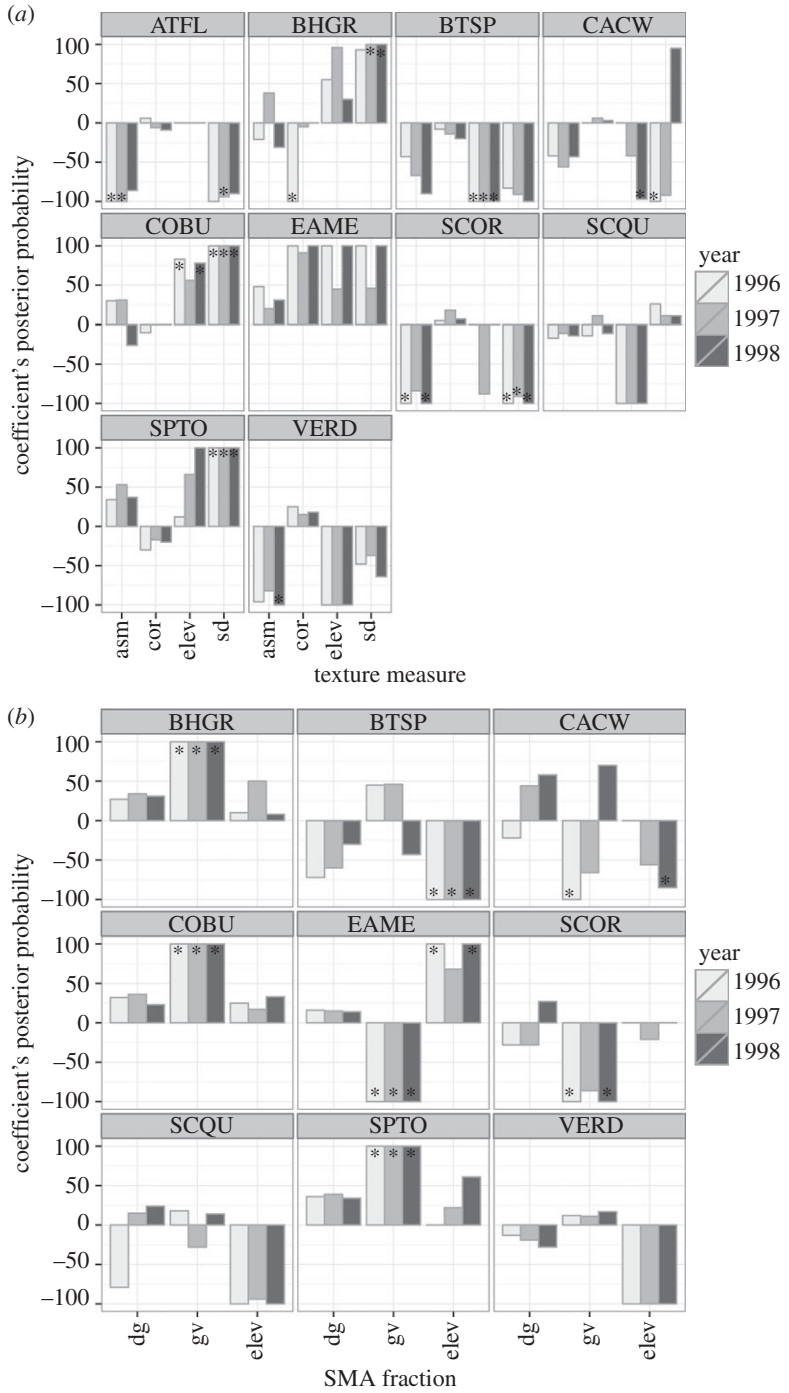

Figure 4. Coefficients' posterior probabilities obtained from the Bayesian model averaging of NDVI texture (*a*), and SMA fractions (*b*) covariates used to explain the abundance or occurrence of birds at all 38 study plots. The amplitude of the bars is indicative of the relative contribution of each variable for explaining the response. Stars indicate variables/year combinations for which a 95% posterior probability interval built around the corresponding BMA coefficient estimate did not include zero. Texture measures acronyms: asm, angular second moment; cor, correlation; elev, elevation; sd, standard deviation. SMA fractions acronyms: dg, dry vegetation; gv, green vegetation.

Among the different SMA fractions, green vegetation was by far the best predictor of bird species richness, and of the abundance of most species. As expected, species richness was higher in areas with higher green vegetation. The abundance of black-headed grosbeak, spotted towhee and common bushtit was consistently higher across the three years of data in areas with a higher amount of green vegetation. In our study site, these species nest either in patches of dense vegetation relative to available vegetation (grosbeak, towhee), or in mature pinyon or juniper trees, which would exhibit a large proportion of greenness in a given pixel. Eastern meadowlark, on the other hand, occurred in all three years in areas of lower green vegetation, typically grasslands.

The association of bird species richness and species abundance with measures of texture confirmed the value of remotely sensed data derived from continuous, unclassified imagery for species distribution modelling [9]. We acknowledge, however, that more research is necessary to understand the full potential, and limitations, of raw imagery for habitat modelling. The dependence of these indices on the area covered by the satellite sensor, or scene, needs to be explored. Phenology, for example, impacts some of the image texture measures more than others [54,55]. Similarly, the degree to which image pre-processing (e.g. topographic and radiometric correction) affects image texture is largely unknown. SMA has the benefit though that it is more consistent across an image,

and potentially several images, than other measures such as NDVI [29]. And while it was outside the goals of our study, further study to understand the differences in predictive power between SMA-based texture and NDVI texture, and SMA values versus NDVI values, are potentially fruitful next steps that may yield further refinements in characterizing habitat for biodiversity.

Ultimately, habitat models need to be built with sound ecological variables in order to be useful for species conservation and management. Our results demonstrated the value of a simple vegetation index, from which we derived image texture, for characterizing bird habitat in the Chihuahuan Desert. The approach we used is applicable to other systems as well. In Argentina, for example, we successfully applied a similar methodology to model the spatial distribution of the greater rheas [23].

Using relationships derived at the plot level, NDVI texture calculated across the whole study area could predict the value of different areas for given species or guilds, or, using species richness, for the entire avian community. The integration of measures of habitat heterogeneity derived from unclassified imagery into habitat models can be applied to other ecosystems as well. Based on our result, we suggest that such an approach will perform particularly well in ecosystems where habitat heterogeneity is an important component of wildlife habitat, and where heterogeneity occurs at a scale that can be detected with satellite imagery.

Acknowledgements. We thank the field assistants who collected bird data between 1996 and 1998. A special thanks to P. A. Townsend for the use of the ADS Fieldspec Pro II spectroradiometer, and to C. Kingdon for his assistance with the spectroradiometer. The spectral mixture analysis was conducted at the Geomatics Lab of Humboldt-Universität zu Berlin. We thank all members of the Geomatics Lab at Humboldt-Universität for their precious feedback, with special thanks to A. Damm and S. van der Linden.

Data accessibility. Data deposited in the Dryad Digital Repository (doi:10.5061/dryad.sk792).

Funding statement. The spectral mixture analysis was partly funded through the Vilas Travel Fellowship by the University of Wisconsin-Madison Graduate School. We acknowledge funding by the Strategic Environmental Research and Development Program and the NASA Biodiversity Program. Support for acquiring bird data was provided by the US Department of Defense Legacy Resource Management Program, Ft Bliss Directorate of Environment, USGS BRD Texas Cooperative Fish and Wildlife Research Unit, USGS BRD Wisconsin Cooperative Wildlife Research Unit, and the Department of Forest and Wildlife Ecology, University of Wisconsin-Madison.

References

1. Nagendra H, Lucas R, Honrado JP, Jongman RHG, Tarantino C, Adamo M, Mairota P. 2013 Remote sensing for conservation monitoring: assessing protected areas, habitat extent, habitat condition, species diversity, and threats. *Ecol. Indic.* **33**, 45–59. (doi:10.1016/j.ecolind.2012.09.014)
2. Nagendra H. 2001 Using remote sensing to assess biodiversity. *Int. J. Remote Sens.* **22**, 2377–2400. (doi:10.1080/01431160117096)
3. Kuemmerle T *et al*. 2010 European Bison habitat in the Carpathian Mountains. *Biol. Conserv.* **143**, 908–916. (doi:10.1016/j.biocon.2009.12.038)
4. Turner W, Spector S, Gardiner N, Fladeland M, Sterling E, Steininger M. 2003 Remote sensing for biodiversity science and conservation. *Trends Ecol. Evol.* **18**, 306–314. (doi:10.1016/S0169-5347(03)00070-3)
5. Estes LD, Reillo PR, Mwangi AG, Okin GS, Shugart HH. 2010 Remote sensing of structural complexity indices for habitat and species distribution modeling. *Remote Sens. Environ.* **114**, 792–804. (doi:10.1016/j.rse.2009.11.016)
6. Hamada Y, Stow DA, Roberts DA, Franklin J, Kyriakidis PC. 2013 Assessing and monitoring semi-arid shrublands using object-based image analysis and multiple endmember spectral mixture analysis. *Environ. Monit. Assess.* **185**, 3173–3190. (doi:10.1007/s10661-012-2781-z)
7. Wood EM, Pidgeon AM, Radeloff VC, Keuler NS. 2013 Image texture predicts avian density and species richness. *PLoS ONE* **8**, e63211. (doi:10.1371/journal.pone.0063211)
8. MacArthur RH. 1972 *Geographical ecology: patterns in the distribution of species*. New York, NY: Harper & Row.
9. Bradley BA, Fleishman E. 2008 Can remote sensing of land cover improve species distribution modelling? *J. Biogeogr.* **35**, 1158–1159. (doi:10.1111/j.1365-2699.2008.01928.x)
10. Lucas NS, Shanmugam S, Barnsley M. 2002 Sub-pixel habitat mapping of a costal dune ecosystem. *Appl. Geogr.* **22**, 253–270. (doi:10.1016/S0143-6228(02)00007-3)
11. Rodriguez-Galiano VF, Chica-Olmo M, Abarca-Hernandez F, Atkinson PM, Jeganathan C. 2012 Random Forest classification of Mediterranean land cover using multi-seasonal imagery and multi-seasonal texture. *Remote Sens. Environ.* **121**, 93–107. (doi:10.1016/j.rse.2011.12.003)
12. Vijayaraghavan R, Sundaramoorthy S. 2012 Mapping *Prosopis juliflora* using satellite data in a part of Indian Thar desert. *Int. J. Ecol. Environ. Sci.* **38**, 9–18.
13. Pesaresi M, Gerhardinger A. 2011 Improved textural built-up presence index for automatic recognition of human settlements in arid regions with scattered vegetation. *IEEE J. Sel. Top. Appl. Earth Obs. Remote Sens.* **4**, 16–26. (doi:10.1109/JSTARS.2010.2049478)
14. Stefanov WL, Ramsey MS, Christensen PR. 2001 Monitoring urban land cover change: an expert system approach to land cover classification of semiarid to arid urban centers. *Remote Sens. Environ.* **77**, 173–185. (doi:10.1016/S0034-4257(01)00204-8)
15. St-Louis V, Pidgeon AM, Clayton MK, Locke BA, Bash D, Radeloff VC. 2009 Satellite image texture and a vegetation index predict avian biodiversity in the Chihuahuan Desert of New Mexico. *Ecography* **32**, 468–480. (doi:10.1111/j.1600-0587.2008.05512.x)
16. Haralick R, Shanmugam K, Dinstein I. 1973 Textural features for image classification. *IEEE Trans. Syst. Man Cybern.* **SMC3**, 610–621. (doi:10.1109/TSMC.1973.4309314)
17. Kushwaha S, Kuntz S, Oesten G. 1994 Applications of image texture in forest classification. *Int. J. Remote Sens.* **15**, 2273–2284. (doi:10.1080/01431169408954242)
18. Franklin SE, Hall RJ, Moskal LM, Maudie AJ, Lavigne MB. 2000 Incorporating texture into classification of forest species composition from airborne multispectral images. *Int. J. Remote Sens.* **21**, 61–79. (doi:10.1080/014311600210993)
19. Coburn CA, Roberts ACB. 2004 A multiscale texture analysis procedure for improved forest stand classification. *Int. J. Remote Sens.* **25**, 4287–4308. (doi:10.1080/0143116042000192367)
20. Puissant A, Hirsch J, Weber C. 2005 The utility of texture analysis to improve per-pixel classification for high to very high spatial resolution imagery. *Int. J. Remote Sens.* **26**, 733–745. (doi:10.1080/01431160512331316838)
21. Jobin B, Labrecque S, Grenier M, Falardeau G. 2008 Object-based classification as an alternative approach to the traditional pixel-based classification to identify potential habitat of the grasshopper sparrow. *Environ. Manage.* **41**, 20–31. (doi:10.1007/s00267-007-9031-0)
22. Hepinstall JA, Sader SA. 1997 Using Bayesian statistics, Thematic Mapper satellite imagery, and breeding bird survey data to model bird species probability of occurrence in Maine. *Photogramm. Eng. Remote Sens.* **63**, 1231–1237.
23. Bellis LM, Pidgeon AM, Radeloff VC, St-Louis V, Navarro JL, Martella MB. 2008 Modeling habitat suitability for greater rheas based on image texture. *Ecol. Appl.* **18**, 1956–1966. (doi:10.1890/07-0243.1)

24. St-Louis V, Pidgeon AM, Radeloff VC, Hawbaker TJ, Clayton MK. 2006 High-resolution image texture as a predictor of bird species richness. *Remote Sens. Environ.* **105**, 299–312. (doi:10.1016/j.rse.2006.07.003)
25. MacArthur R, MacArthur J. 1961 On bird species diversity. *Ecology* **42**, 594. (doi:10.2307/1932254)
26. Shimabukuro Y, Smith J. 1991 The least-square mixing models to generate fraction images derived from remote-sensing multispectral data. *IEEE Trans. Geosci. Remote Sens.* **29**, 16–20. (doi:10.1109/36.103288)
27. Roberts DA, Gardner M, Church R, Ustin S, Scheer G, Green RO. 1998 Mapping chaparral in the Santa Monica mountains using multiple endmember spectral mixture models. *Remote Sens. Environ.* **65**, 267–279. (doi:10.1016/S0034-4257(98)00037-6)
28. Sonnenschein R, Kuemmerle T, Udelhoven T, Stellmes M, Hostert P. 2011 Differences in Landsat-based trend analyses in drylands due to the choice of vegetation estimate. *Remote Sens. Environ.* **115**, 1408–1420. (doi:10.1016/j.rse.2011.01.021)
29. Elmore AJ, Mustard JF, Manning SJ, Lobell DB. 2000 Quantifying vegetation change in semiarid environments: precision and accuracy of spectral mixture analysis and the Normalized Difference Vegetation Index. *Remote Sens. Environ.* **73**, 87–102. (doi:10.1016/S0034-4257(00)00100-0)
30. Hostert P, Roder A, Hill J, Udelhoven T, Tsiourlis G. 2003 Retrospective studies of grazing-induced land degradation: a case study in central Crete, Greece. *Int. J. Remote Sens.* **24**, 4019–4034. (doi:10.1080/0143116031000103844)
31. Estes LD, Okin GS, Mwangi AG, Shugart HH. 2008 Habitat selection by a rare forest antelope: a multi-scale approach combining field data and imagery from three sensors. *Remote Sens. Environ.* **112**, 2033–2050. (doi:10.1016/j.rse.2008.01.004)
32. Bino G, Levin N, Darawshi S, Van Der Hal N, Reich-Solomon A, Kark S. 2008 Accurate prediction of bird species richness patterns in an urban environment using Landsat-derived NDVI and spectral unmixing. *Int. J. Remote Sens.* **29**, 3675–3700. (doi:10.1080/01431160701772534)
33. Pasher J, King D, Lindsay K. 2007 Modelling and mapping potential hooded warbler (*Wilsonia citrina*) habitat using remotely sensed imagery. *Remote Sens. Environ.* **107**, 471–483. (doi:10.1016/j.rse.2006.09.022)
34. Pidgeon AM, Radeloff VC, Mathews NE. 2003 Landscape-scale patterns of black-throated sparrow (*Amphispiza bilineata*) abundance and nest success. *Ecol. Appl.* **13**, 530–542. (doi:10.1890/1051-0761(2003)013[0530:LSPOBT]2.0.CO;2)
35. Pidgeon AM, Mathews NE, Benoit R, Nordheim EV. 2001 Response of avian communities to historic habitat change in the northern Chihuahuan Desert. *Conserv. Biol.* **15**, 1772–1788. (doi:10.1046/j.1523-1739.2001.00073.x)
36. U.S. Department of Agriculture Natural Resources Conservation Service 1996 Fort Bliss soils.
37. Kuemmerle T, Roeder A, Hill J. 2006 Separating grassland and shrub vegetation by multidate pixel-adaptive spectral mixture analysis. *Int. J. Remote Sens.* **27**, 3251–3271. (doi:10.1080/01431160500488944)
38. Chander G, Markham B. 2003 Revised Landsat-5 TM radiometric calibration procedures and postcalibration dynamic ranges. *IEEE Trans. Geosci. Remote Sens.* **41**, 2674–2677. (doi:10.1109/TGRS.2003.818464)
39. Markham BL, Barker JL. 1986 *Landsat MSS and TM post-calibration dynamic ranges, exoatmospheric reflectances and at-satellite temperatures*. EOSAT Technical Notes 1. Lanham, MD: EOSAT.
40. Tanré D, Deroo C, Duhaut P, Herman M, Morcrette J, Perbos J, Deschamps P. 1990 Description of a computer code to simulate the satellite signal in the solar spectrum - the 5S code. *Int. J. Remote Sens.* **11**, 659–668. (doi:10.1080/01431169008955048)
41. Baldridge A, Hook S, Grove C, Riviera G. 2009 The ASTER spectral library version 2.0. *Remote Sens. Environ.* **113**, 711–715. (doi:10.1016/j.rse.2008.11.007)
42. ERDAS. 1999 *Erdas Field Guide*. Atlanta, GA: Erdas.
43. Smith M, Ustin S, Adams J, Gillepsie A. 1990 Vegetation in deserts: 1. A regional measure of abundance from multispectral images. *Remote Sens. Environ.* **31**, 1–26. (doi:10.1016/0034-4257(90)90074-V)
44. Clark R, Swayze G, Wise R, Livo E, Hoefen T, Kokaly R, Sutley S. 2007 USGS digital spectral library splib06a. U.S. Geological Survey, Data Series 231. Reston, Virginia: USGS. See http://speclab.cr.usgs.gov/spectral-lib.html.
45. Small C. 2004 The Landsat ETM plus spectral mixing space. *Remote Sens. Environ.* **93**, 1–17. (doi:10.1016/j.rse.2004.06.007)
46. Garcia-Haro FJ, Sommer S, Kemper T. 2005 A new tool for variable multiple endmember spectral mixture analysis (VMESMA). *Int. J. Remote Sens.* **26**, 2135–2162. (doi:10.1080/01431160512331337817)
47. St-Louis V, Pidgeon AM, Clayton MK, Locke BA, Bash D, Radeloff VC. 2010 Habitat variables explain loggerhead shrike occurrence in the northern Chihuahuan Desert, but are poor correlates of fitness measures. *Landsc. Ecol.* **25**, 643–654. (doi:10.1007/s10980-010-9451-8)
48. Raftery AE. 1995 Bayesian model selection in social research. *Sociol. Methodol.* **25**, 111–163. (doi:10.2307/271063)
49. Link WA, Barker RJ. 2006 Model weights and the foundations of multimodel inference. *Ecology* **87**, 2626–2635. (doi:10.1890/0012-9658(2006)87[2626:MWATFO]2.0.CO;2)
50. R Core Team. 2013 *R: a language and environment for statistical computing*. Vienna, Austria: R Foundation for Statistical Computing.
51. Pinheiro J, Bates D, DebRoy S, Sarkar D, R Development Core Team. 2013 *nlme: Linear and nonlinear mixed effects models*. Vienna, Austria: R Foundation for Statistical Computing.
52. Hurlbert AH. 2004 Species–energy relationships and habitat complexity in bird communities. *Ecol. Lett.* **7**, 714–720. (doi:10.1111/j.1461-0248.2004.00630.x)
53. Huete A. 1988 A soil-adjusted vegetation index (SAVI). *Remote Sens. Environ.* **25**, 295–309. (doi:10.1016/0034-4257(88)90106-X)
54. Culbert PD, Pidgeon AM, St-Louis V, Bash D, Radeloff VC. 2009 The impact of phenological variation on texture measures of remotely sensed imagery. *IEEE J. Sel. Top. Appl. Earth Obs. Remote Sens.* **2**, 299–309. (doi:10.1109/JSTARS.2009.2021959)
55. Culbert PD, Radeloff VC, St-Louis V, Flather CH, Rittenhouse CD, Albright TP, Pidgeon AM. 2012 Modeling broad-scale patterns of avian species richness across the Midwestern United States with measures of satellite image texture. *Remote Sens. Environ.* **118**, 140–150. (doi:10.1016/j.rse.2011.11.004)